JMB

Available online at www.sciencedirect.com

ScienceDirect

ELSEVIER

COMMUNICATION

Solution and Crystal Structures of mRNA Exporter Dbp5p and Its Interaction with Nucleotides

Jing-Song Fan[1]†, Zhihong Cheng[2]†, Jingfeng Zhang[1]†, Christian Noble[2], Zhihong Zhou[2], Haiwei Song[1,2]* and Daiwen Yang[1]*

[1]*Department of Biological Sciences, National University of Singapore, 14 Science Drive 4, Singapore 117543, Singapore*

[2]*Institute of Molecular and Cell Biology, 61 Biopolis Drive, Proteos, Singapore 138673, Singapore*

DEAD-box protein 5 (Dbp5p) plays very important roles in RNA metabolism from transcription, to translation, to RNA decay. It is an RNA helicase and functions as an essential RNA export factor from nucleus. Here, we report the solution NMR structures of the N- and C-terminal domains (NTD and CTD, respectively) of Dbp5p from *Saccharomyces cerevisiae* (ScDbp5p) and X-ray crystal structure of Dbp5p from *Schizosaccharomyces pombe* (SpDbp5p) in the absence of nucleotides and RNA. The crystal structure clearly shows that SpDbp5p comprises two RecA-like domains that do not interact with each other. NMR results show that the N-terminal flanking region of ScDpbp5 (M1-E70) is intrinsically unstructured and the region Y71–R121 including the Q motif is highly dynamic on millisecond–microsecond timescales in solution. The C-terminal flanking region of ScDbp5p forms a short β-strand and a long helix. This helix is unique for ScDbp5p and has not been observed in other DEAD-box proteins. Compared with other DEAD-box proteins, Dbp5p has an extra insert with six residues in the CTD. NMR structure reveals that the insert is located in a solvent-exposed loop capable of interacting with other proteins. ATP and ADP titration experiments show that both ADP and ATP bind to the consensus binding site in the NTD of ScDbp5p but do not interact with the CTD at all. Binding of ATP or ADP to NTD induces significant conformational rearrangement too.

© 2009 Elsevier Ltd. All rights reserved.

Edited by M. F. Summers   *Keywords:* DEAD-box protein; NMR; X-ray; Dbp5p; protein structure

---

DEAD-box protein 5 (Dbp5p), also named Rat8p, is an RNA helicase[1] and functions as an essential mRNA export factor.[2–4] It shuttles between the nucleus and cytoplasm in an Xpo1p-dependent manner.[5] Dbp5p is mainly localized in the cytoplasm and is recruited to the nuclear rim by nucleoporin Nup159p/Rat7p[6] and associated with Gle1p/Rss1p, Rip1p/Nup42p, Ymr255p/Gfd1p, and Zds1 on the cytoplasmic fibril of NPC.[7] It is proposed that Dbp5p

plays an important role in mRNA export by displacing Mex67p from exported mRNA–protein particles.[8] Recent works show that Dbp5p participates in translation termination and mRNA turnover in cytoplasm through the interactions with release factors eRF1 and eRF3, polyadenlyate-binding protein Pab1,[9] and the P-body components.[10] Other works show that Dbp5p remains enzymatically inactive until mRNA–protein particles reach the cytoplasmic NPC face, where the ATPase activity of Dbp5p is greatly stimulated by nucleoporin Gle1p together with inositol polyphosphate InsP$_6$.[11,12] Thus, the activation of Dbp5p may provide an input of energy to drive the removal of critical mRNA binding proteins. The interactions of Dbp5p with RNA and other proteins are crucial for transcription initiation, mRNA export, and translation termination. However, the molecular mechanism by which Dbp5p regulates these processes remains unclear.

The three-dimensional (3D) structures are available for a number of DEAD-box proteins with or

---

Corresponding authors. E-mail addresses: dbsydw@nus.edu.sg; haiwei@imcb.a-star.edu.sg.

† J.-S.F., Z.C., and J.Z. contributed equally to this work.

Abbreviations used: HSQC, heteronuclear single quantum correlation; CTD, C-terminal domain; Dbp5p, DEAD-box protein 5; NTD, N-terminal domain; ScDbp5p, Dbp5p from *Saccharomyces cerevisiae*; SpDbp5p, from *Schizosaccharomyces pombe*; 3D, three-dimensional; PDB, Protein Data Bank; NOE, nuclear Overhauser enhancement.

without their corresponding binding partners, including MjDEAD from *Methanococcus jannaschii*[13], human splicing factor UAP56,[14] yeast initiation factor eIF4A[15] and yeast mRNA translation and degradation factor Dhh1p,[16] *Drosophila* VASA,[17] human DEAD-box helicase DDX3X,[18] and human DEAD-box helicase DDX19 [HuDbp5p, a human homolog of Dbp5p; Protein Data Bank (PDB) code: 3EWS]. The structures of isolated N-terminal domains (NTDs) of several proteins (yeast eIF4A, human UAP56, *Dugesia japonica* VASA-like gene B protein, BstDEAD, and *Thermus thermophilus* Hera helicase) have also been determined by X-ray crystallography,[19–24] while the C-terminal domain (CTD) structures of human UAP56 and a closely related family DEAH NS3 helicase have been solved recently by X-ray and NMR, respectively.[21,25] Nevertheless, the 3D structure of the full-length Dbp5p or individual Dbp5p domains is still unavailable in the absence of nucleotides and in the presence of RNA, hampering its further mechanistic studies.

Dbp5p from *Saccharomyces cerevisiae* (ScDbp5p) consists of 482 residues with a molecular mass of ~53 kDa. Its sequence identities with other DEAD-box proteins whose 3D structures have been determined range from ~22% with *Drosophila* VASA to

~47% with HuDbp5p. Dbp5p from *Schizosaccharomyces pombe* (SpDbp5p) contains 503 residues. It shares ~56% and ~51% sequence identities with ScDbp5p and human HuDbp5p, respectively. Despite the conservation of key residues in the structural core of the DEAD-box proteins, the flanking N- and C-terminal sequences of Dbp5p are very different from those of other DEAD-box proteins, which are thought to provide additional interactions with its substrates or cofactors. Given the multiple functional roles that Dbp5p plays in the RNA life cycle, it is important to solve its 3D structure to understand how it functions. Here, we report the solution NMR structures of the NTD and CTD of ScDbp5p and the X-ray crystal structure of full-length SpDbp5p in the absence of nucleotides. Taking the advantage of NMR backbone assignments, we investigated the binding property of the NTD and CTD with nucleotides (ADP and ATP) using NMR titration experiments.

NMR structure determination of NTD and CTD of ScDbp5p

Several dozens of intense peaks were found in the heteronuclear single quantum correlation (HSQC)

Table 1. Structural statistics for the NTD and CTD of ScDbp5p

	NTD[a]	CTD[a]
All NOE distance restraints[b]	2146	1825
Intraresidues	817	727
Interresidue, sequential ($|i-j|=1$)	603	556
Interresidue, medium range ($1<|i-j|<5$)	288	247
Interresidue, long range ($|i-j|\geq5$)	438	295
Hydrogen-bond restraints	57	53
Dihedral angle restraints (ϕ,φ)[c]	184	201
Deviations from idealized covalent geometry[d]		
RMSD of bond lengths (Å)	0.0028±0.00005	0.0029±0.00005
RMSD of bond angles (°)	0.407±0.06	0.388±0.01
RMSD of improper angles (°)	0.350±0.0097	0.324±0.0098
Deviations from experimental restraints		
RMSD of distance restraints (Å)	0.0323±0.0009	0.0369±0.0008
RMSD of dihedral angle restraints (°)	0.452±0.064	0.567±0.076
Ramachandran plot analysis (%)[e]		
Residues in favored region	64.1	66.3
Residues in additional allowed regions	27.8	24.8
Residues in generally allowed regions	6.9	7.2
Residues in disallows disallowed regions	1.2	1.7
Average RMSD from mean structure (Å)[f]		
All residues	1.42±0.25	1.54±0.27
Regular 2° structure region	0.86±0.17	1.10±0.21

[a] His$_6$-tag-fused recombinant ^{15}N,^{13}C-labeled NTD and CTD were expressed in *Escherichia coli* using M9 medium containing 1 g/l ^{15}NH$_4$Cl and 2 g/l of [^{13}C]-glucose as the sole nitrogen and carbon source, respectively, at 20 °C. The proteins were purified first using a Ni-NTA affinity column and then using a Superdex-100 gel-filtration column (Amersham Pharmacia Biotech) after the cleavage of His$_6$-tag by thrombin. The purified proteins were concentrated to about 0.6 mM in a buffer containing 20 mM 4-morpholineethanesulfonic acid (pH 6.7), 100 mM KAc, and 0.1% 2-mercaptoethanol for NMR measurements.

[b] All NMR experiments were performed on a Bruker AVANCE 800 spectrometer equipped with a TXI cryoprobe at 25 °C. The NMR experiments used on each sample are 2D HSQC, 3D TROSY (transverse relaxation optimized spectroscopy)-HNCA, 3D MQ-CCH-TOCSY (total correlated spectroscopy),[34,35] and 4D ^{13}C,^{15}N time-shared NOESY (NOE spectroscopy).[26,27] All data were processed with NMRPipe[36] and analyzed with SPARKY.[37] The distance restraints were obtained by classifying the NOE cross peaks into three categories: strong (1.8–2.9 Å), medium (1.8–3.5 Å), and weak (1.8–5.0 Å). Solution structures of NTD and CTD were calculated using the torsion angle dynamics simulated annealing method within XPLOR-NIH.[38]

[c] Dihedral angles of backbone ϕ and ψ were predicted by TALOS[28] using the chemical shifts of C$^{\alpha}$, C$^{\beta}$, H$^{\alpha}$, N, and HN.

[d] Twenty lowest-energy conformers with no NOE violations greater than 0.5 Å and no torsion angle violations greater than 5° were selected from 100 conformers to represent the NMR ensembles.

[e] Calculated with PROCHECK-NMR.[39]

[f] Calculated with MOLMOL[40]; averages are over backbone atoms.

spectra of full-length ScDbp5p and its NTD (residues M1–T296) samples. Backbone resonance assignments confirm that the intense peaks are from the N-terminal flanking region within residues M1–E70. Further analysis indicates that those residues adopt an unstructured conformation and have no interaction with other parts of the protein (data not shown). Hence, an N-terminal truncated fragment (residues Y71–T296) was chosen for structural determination of the NTD of ScDbp5p.

The backbone and side-chain chemical shift assignments were obtained using the strategy recently developed in our laboratory.[26,27] For the NTD, 26 residues did not yield observable HSQC signals. These residues are located mainly in the N-terminal region, including Y71–L77, D79, L88–A91, F94, E96, K111, F112, K117, Q119–R121, Q137, and S138. This result indicates that the N-terminal region (Y71–R121) is quite dynamic on millisecond–microsecond timescales. C-terminal residues T291–Q295 could not be observed either in the HSQC spectrum, very likely due to conformational exchanges at the C-terminal end. For the CTD, only six residues (T329, K340, G362, L390, A411, and K443) did not give rise to expected HSQC signals, implying that the CTD is much less dynamic than

the NTD on millisecond–microsecond timescales. Using assigned nuclear Overhauser enhancement (NOE) peaks as distance constraints, together with dihedral angle constraints derived from TALOS,[28] we determined the solution structures of both the NTD and CTD by NMR methods (Table 1).

The structures of the NTD and CTD are well defined except for two regions (residues Y71–A91 and K111–L127) in the NTD (Fig. 1). The root-mean-square deviations (RMSDs) for backbone atoms (N, C^α, C′, and CO) in regular secondary-structure regions among 20 lowest energy conformers were 0.86 ± 0.17 Å and 1.10 ± 0.21 Å for the NTD and CTD, respectively. The ribbon diagrams show that both the CTD and NTD adopt a RecA-like fold with an α/β-structure[29] (Fig. 2a and b). CTD comprises seven parallel β-strands (β7/β1/β6/β5/β2/β4/β3) surrounded by three helices on one side and three helices on the other (Fig. 2a), while NTD also consists of seven parallel β-strands (β7/β1/β6/β5/β2/β4/β3) but surrounded by six helices on one side and four helices on the other (Fig. 2b). Although the NTD and CTD share only ~10% sequence identities, their tertiary structures are quite similar with a mean RMSD value of 1.8 Å over 71 C^α atoms.
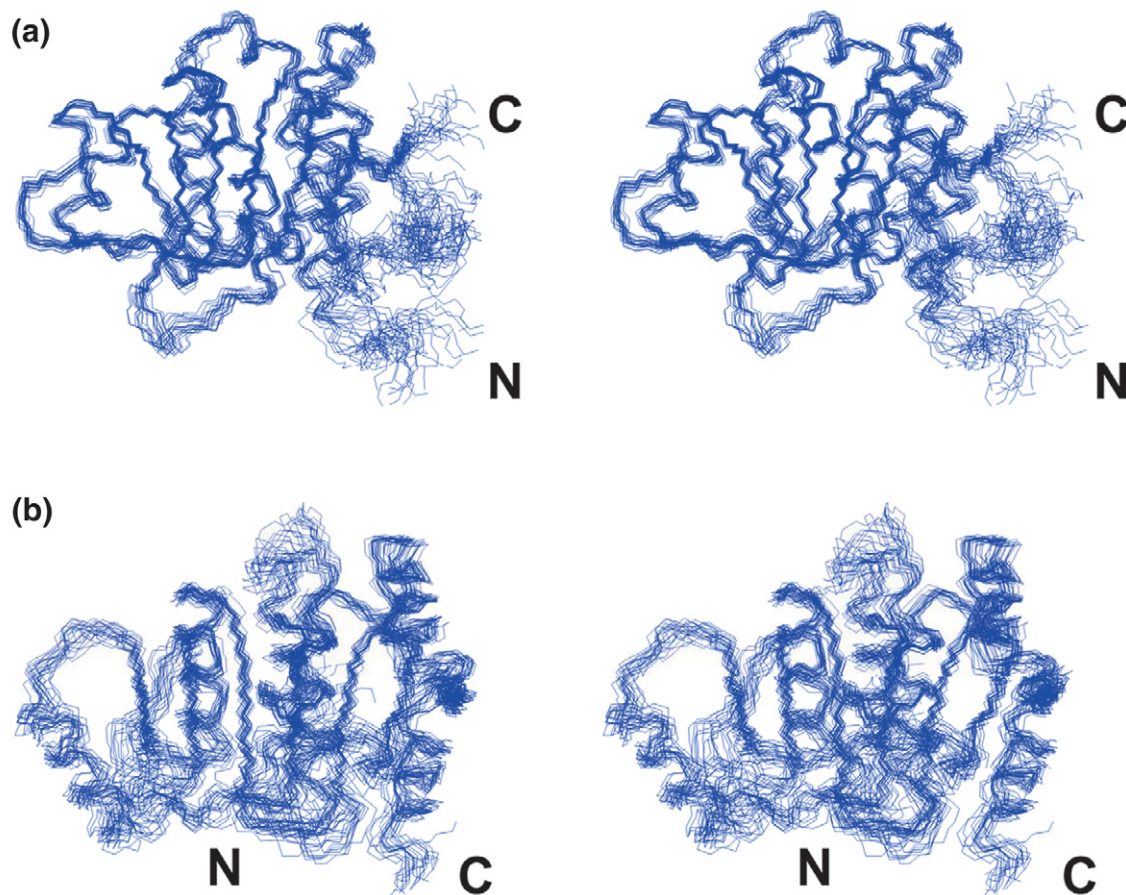
Fig. 1. Stereo views of 20 superimposed accepted structures for NTD and CTD of ScDbp5p. The figure was generated using MOLMOL.[40] Only backbone atoms (N, C^α, C′, and CO) were chosen to superimpose the structures. (a) The region from Q81 to T296 was drawn to represent the NTD structure. (b) The region from T296 to D482 was drawn to represent the CTD structure.

X-ray structure determination of SpDbp5p

The crystal structure of SpDbp5p (residues 139–481) was determined at a resolution of 2.8 Å in the absence of nucleotides (Table 2). Several regions of the polypeptide chain including the N- and C-terminal regions (residues 1–138 and 482–503), four residues in the flexible linker region between NTD and CTD (residues 321–324), and some of the loop regions (residues 218–227, 270–271, 349–350, 384–
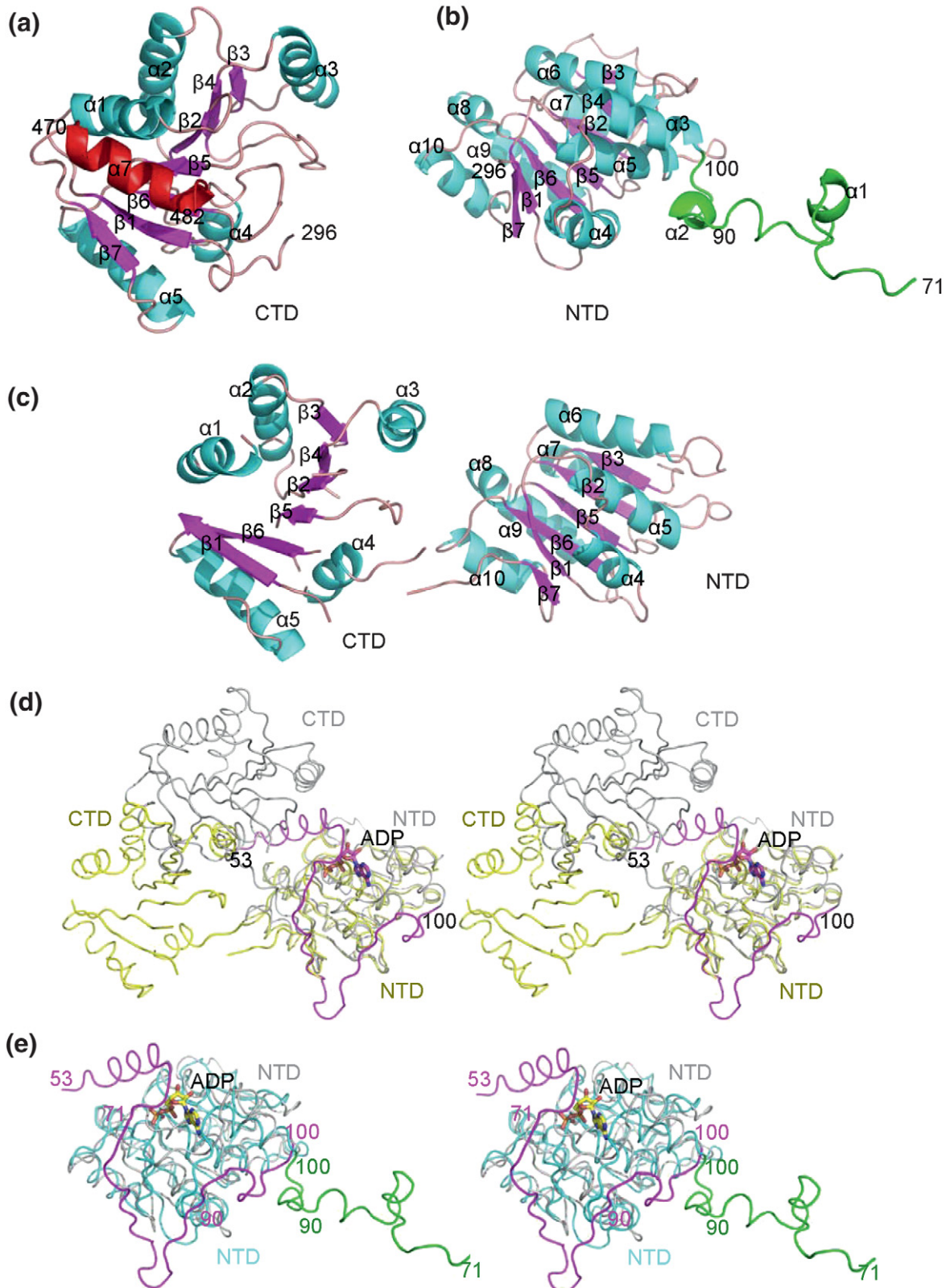
Fig. 2 (*legend on next page*)

388, 411–415, 427–430, and 433–437) were not visible in the electron density map and were assumed to be disordered. The polypeptide chain of SpDbp5p is folded into two α/β-domains, each with a RecA-like topology as observed in other DEAD-box proteins (Fig. 2c). The NTD is composed of a parallel, seven-stranded β-sheet flanked by three helices on one side and four helices on the other. The CTD is also a parallel α/β-structure but with three helices on one side and two helices on the other, surrounding the central, seven-stranded β-sheet. The NTD is connected to the CTD by a short stretch of peptide, making the whole molecule resemble a dumbbell with no interactions at all between the two domains.

Comparison of Dbp5p and DEAD-box protein structures

Structural comparison shows that the individual domain structures among SpDbp5p, ScDbp5p, and HuDbp5p in an ADP-bound state (HuDbp5p-ADP) are similar to one another with mean pairwise C^{α} RMSD values of 1.2–1.95 Å (Supplementary Table S1). The structural similarities in the conserved helicase motifs are consistent with the sequence similarities of the three Dbp5p proteins (Supplementary Fig. S1). Dbp5p and other DEAD-box proteins share relatively low sequence identity, but the structure similarity in the conserved core regions between different Dbp5ps is comparable to that between Dbp5p and other DEAD-box proteins (Supplementary Table S1). In all the structures, the arrangement of the seven parallel β-strands is the same; except for the flexible motif Q, the conserved motifs (I, II, Ia, Ib, III, IV, V, and VI) adopt a similar conformation. Despite the structural similarities of the individual domains, the relative orientation of NTD with respect to CTD differs significantly between DEAD-box proteins. For instance, the orientation of the CTD between SpDbp5p and HuDbp5p differs by ∼27° when the NTD is superimposed. Because of the high sequence similarity between SpDbp5p and HuDbp5p, the structure of HuDbp5p in the absence of ADP may resemble the structure of SpDbp5p. Therefore, it is very likely that ADP binding induced a large conformational change of Dbp5p (Fig. 2d). Moreover, when the NTD of SpDbp5p is superimposed with that of Vasa, the relative orientation change of CTD of SpDbp5p with respect to that of Vasa is ∼5° in rotation and 30 Å in translation. Importantly, the residues involved in

the Vasa NTD–CTD interface are conserved in Vasa and SpDbp5p (e.g., Q161, G163, E195, L196, E262, A294, T295, D438, and H444 in SpDbp5p numbering), suggesting that SpDbp5p and Vasa may adopt a similar conformation upon binding to ATP and RNA. The variation in domain–domain orientation (e.g., ∼5° for Vasa and 27° for HuDbp5p relative to SpDbp5p) reflects the flexibility of the linker region of DEAD-box proteins and the weak domain–domain interactions in the absence of their binding partners. The flexibility is probably important for the protein activity and selectivity.[30]

In addition to the large domain–domain orientation difference between SpDbp5p and HuDbp5p, the N-terminal flanking region (residues 53–100) of HuDbp5p-ADP, which adopts a largely extended conformation in ScDbp5p and SpDbp5p (Fig. 2b), wraps around the body of NTD with some unique structural features. First, the middle part of this flanking region (E78–L80) forms a strand, antiparallel with the outmost strand of the central β-sheet, while the extreme N-terminal region (residues 55–67) is folded into a helix that just positions between the NTD and CTD and interacts with the CTD (Fig. 2e). Second, the C-terminal end of this helix and the loop connecting to the C-terminus of this helix interact with the bound ADP. The structural differences in the flanking region between SpDbp5p and HuDbp5p probably result from the binding of nucleotides.

The structures for the regions from Y71–A91 and K111–L127 in the NTD of ScDbp5p were poorly determined due to the many residues in this region producing unobservable amide resonances. According to the chemical shifts of several assigned residues in the region of Y71–A91, this region may adopt a helical structure. In solution, this region is dynamic on the millisecond–microsecond timescale and may have weak interaction with other regions of the protein. The corresponding region in SpDbp5p is not available, but this region in HuDbp5p is a long unstructured loop (Fig. 2e), consistent with our results. Deletion of residues Y71–S90 rendered the truncated protein (A91–T296) less stable and reduced the binding affinity of the NTD of ScDbp5p to Nup159 (data not shown). A previous study demonstrated that the N-terminal flanking region (residues M1–A122) alone does not bind to Nup159, but the region within residues I80–A122 is necessary for the entire NTD of ScDbp5p to interact with Nup159.[5] Therefore, the dynamics and mobility of the region of Y71–RA122 may be important for Dbp5p to interact with different binding partners.

Fig. 2. NMR and crystal structures of Dbp5p proteins. (a) NMR structure of CTD of ScDbp5p. α-helices and β-strands are colored cyan and magenta, respectively. The extreme C-terminal helix in CTD is shown in red. The first residue number of CTD is 296. (b) NMR structure of NTD of ScDbp5p. The color coding is the same as that in (a) with the exception that the N-terminal extension region is shown in green. (c) Overall structure of SpDbp5p solved by X-ray chromatography. The color coding is the same as that in (a). (d) Stereo view of superposition of SpDbp5p and HuDbp5p-ADP at the NTD. SpDbp5p is colored yellow and HuDbp5p-ADP is in gray, with its N-terminal region in magenta and the bound ADP in stick model. (e) Stereo view of superposition of the NTD of ScDbp5p with that of HuDbp5p-ADP. The N-terminal extension regions with residue numbers from 71 to 100 in ScDbp5p and from 53 to 100 in HuDbp5p are shown in green and magenta, respectively. The positions of residues 71 and 90 are also labeled.

Table 2. Data collection and refinement statistics of SpDbp5p

Data collection[a]	
Wavelength (Å)	0.9725
Resolution limit (Å)	2.8
Space group	C2
Cell parameters	
$a/b/c$ (Å)	108.7/144.0/79.1
$\alpha/\beta/\gamma$ (°)	90/89.9/90
Unique reflections (*n*)	29,528
I/σ	7.2 (2.1)
Completeness (%)	98.5(98.5)
R_{merge}[b]	0.064(0.343)
Refinement statistics[c]	
Data range (Å)	20–2.8
Used reflections (*n*)	28,004
Nonhydrogen atoms	4771
R_{cryst} (%)[d]	28.9
R_{free} (%)[e]	32.7
RMSD	
Bond length (Å)	0.0107
Bond angles (°)	1.359
Ramachandran plot (%)	
Allowed (% residues)	97.5
Generously allowed	2.1
Disallowed	0.4

Values in parentheses indicate the specific values in the highest-resolution shell.

The full-length Dbp5p from *S. pombe* (SpDpb5p) was cloned into the pGEX-6P-1 vector (Amersham) and expressed as a glutathione *S*-transferase fusion protein in *E. coli* BL21 strain. The fusion protein was purified by glutathione affinity column. The glutathione *S*-transferase was removed by PreScission Protease. SpDbp5p was further purified using MonoQ and Superdex-200 gel-filtration columns (Amersham). The eluted protein was concentrated to ~15 mg/ml for crystallization.

[a] Crystallization was performed using the hanging-drop vapor diffusion method at 15 °C. An equal volume of protein sample was mixed with the crystallization solution [100 mM Tris, pH 8.0, 200 mM Ca(Ac)$_2$, and 8.5–10% polyethylene glycol 4000]. Single crystals were transferred by gradually increasing the concentration of ethylene glycol up to 15% in crystallization solution and fast frozen in liquid nitrogen. Crystals belong to the space group C2 with cell parameters $a=108.7$ Å, $b=144.0$ Å, $c=79.1$ Å, and $\beta=89.96°$ and contain two molecules per asymmetric unit. X-ray data were collected at the European Synchrotron Radiation Facility, ID29, and processed with MOSFLM (CCP4).[41]

[b] $R_{merge}=\sum|I_j-\langle I\rangle|/\sum I_j$, where I_j is the intensity of an individual reflection and $\langle I\rangle$ is the average intensity of that reflection.

[c] The structure of SpDbp5p was determined by molecular replacement using the program Phaser.[42] The NTD and CTD of human eIF4A from the EJC complex were taken as the search model. The diffraction data were first processed with space group C2221 with one molecule in asymmetric unit. The NTD and CTD of human eIF4A were found sequentially with Z scores of 9.5 and 8.1, respectively. The resultant model comprising both NTD and CTD was taken as a search model against the data reprocessed with space group C2. Two copies of NTD/CTD were found by Phaser[42] with Z scores of 18.4 and 14.6, respectively, which confirmed that the previous solution was correct. The model was manually rebuilt using Coot.[42] Further crystallographic refinement was performed using REFMAC5[43] with tight noncrystallographic symmetry restraints.

[d] $R_{cryst}=\sum||F_o|-|F_c||/\sum|F_c|$, where F_o denotes the observed structure factor amplitude and F_c denotes the structure factor amplitude calculated from the model.

[e] R_{free} is the same as for R_{cryst} but calculated with 5.0% of randomly chosen reflections omitted from the refinement.

The C-terminal flanking region of ScDbp5p (T462–D482) forms a short β-strand and a long helix. This helix is unique for ScDbp5p since SpDbp5p, HuDbp5p, and other DEAD-box proteins have no such a structural element (Fig. 2a). When it was deleted, the protein became unstable (data not shown). Our NMR structure shows that when the C-terminal flanking region is removed, a large hydrophobic patch will be exposed. This explains why this region is necessary for the stability of the protein. Its functional role is still unclear and needs to be investigated in the future.

Compared with other DEAD-box proteins, Dbp5p and its orthologs have an extra insert with six residues between β5 and α4 in CTDs (e.g., N412–P417 in ScDpb5p and A434–P439 in SpDbp5p). It was suggested that this insert enhances the ability of Dbp5p to export mRNA under heat shock condition.[31] In the eIF4AIII of the EJC complex, the residues surrounding the corresponding insert are involved in binding to Mago and Btz.[32] Our NMR structure shows that this insert is located in the loop region pointing outward and is capable of interacting with unidentified binding partners under certain conditions.

Interactions between ScDbp5p and nucleotides

ScDbp5p and SpDbp5p, like other DEAD-box proteins, contain nine conserved helicase motifs. The most recently solved crystal structures of *Drosophila* VASA and eIF4AIII in the EJC complex reveal that motif Q forms strong interactions with the adenine moiety of AMPPNP, motif I directly interacts with the triphosphate moiety, and motif II interacts with the triphosphate moiety through an Mg^{2+} ion and water molecules.[17,32,33] In addition, motifs V and VI in CTD interact with the triphosphate moiety too, while motifs Ia, Ib, IV, and V are involved in RNA binding.[17,32,33] Similarly, the crystal structure of HuDbp5p-ADP shows that motif Q directly binds the adenine moiety of ADP and motif I directly interacts with the diphosphate moiety of ADP. However, motif II in the NTD and motifs V and VI in the CTD of HuDbp5p do not interact with ADP at all. Interestingly, the N-terminal flanking region is involved in the interaction with ADP, different from other DEAD-box proteins.

In order to investigate the binding of CTD and NTD of ScDbp5p to nucleotides, we carried out NMR titration experiments using ADP and ATP. When 0.1 mM ^{15}N-labeled CTD (residues T296–D482) was titrated with ADP and ATP, no chemical shift change or peak disappearance occurred, suggesting that the CTD alone cannot bind to nucleotides although it shows interactions with nucleotides in the full-length VASA and eIF4AIII in the EJC complex.[17,32] The observation that CTD is not involved in nucleotide binding is consistent with the crystal structure of HuDbp5p-ADP, which shows that ADP binds to the pocket formed exclusively by the residues in the NTD including the residues in the N-terminal flanking region (Figs. 2d and e).
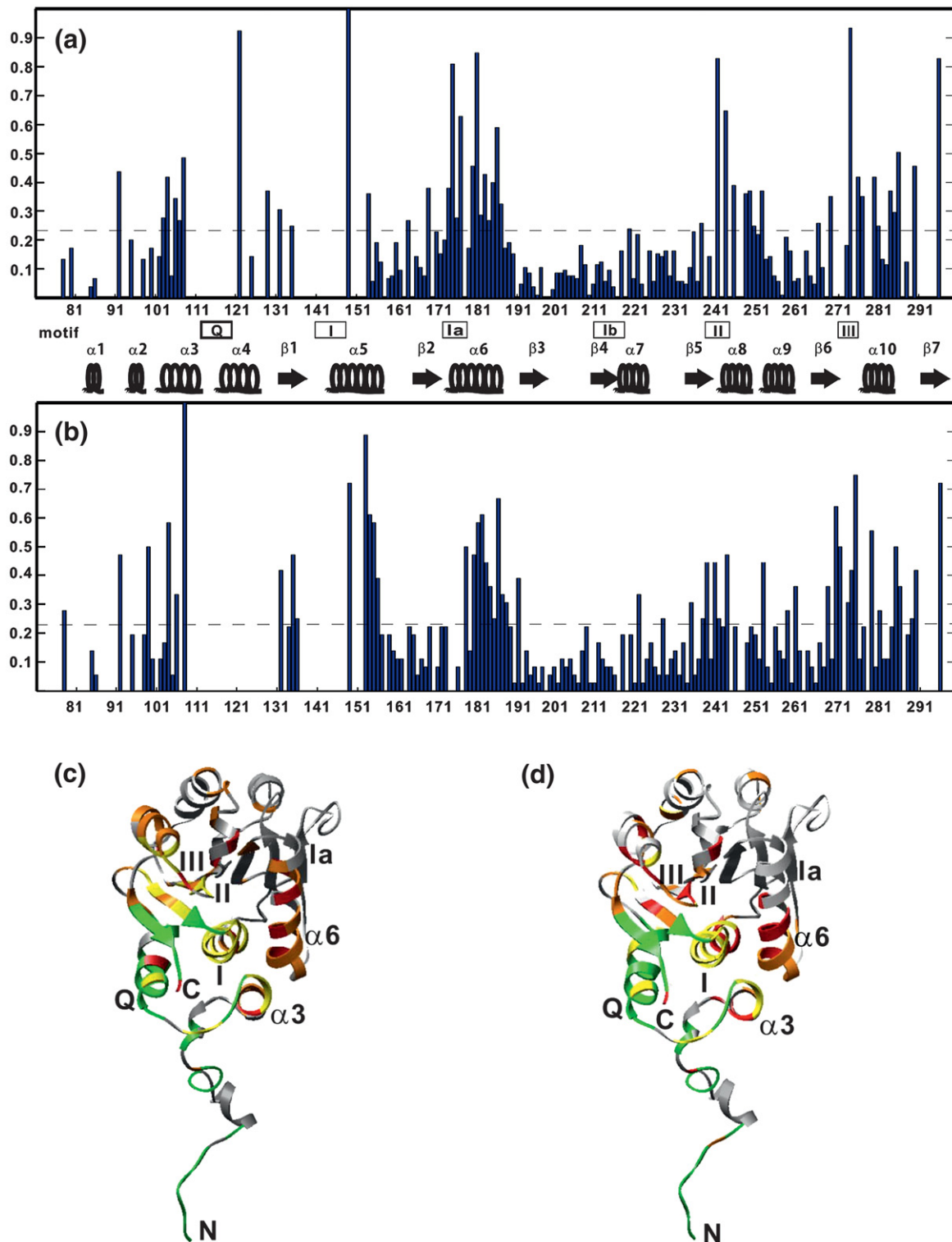
Fig. 3. Normalized combined chemical shift perturbation (Δ_{av}/Δ_{max}) of the NTD of ScDbp5p with ADP (a) and ATP (b). $\Delta_{av} = [(\Delta\delta_{NH}^2 + \Delta\delta_N^2/25)/2]^{1/2}$, where $\Delta\delta_{NH}$ and $\Delta\delta_N$ are the chemical shift difference of amides ^1H and ^{15}N between the samples, in the presence of 3.9 mM ligand and in the absence of ligand, and Δ_{max} is the maximal Δ_{av} value observed. In the empty regions, the HSQC peaks of the residues are either invisible or unassigned. The dotted line represents the mean Δ_{av}/Δ_{max} value over all available residues. The conserved motifs and secondary structural elements are shown in the middle of the two panels. Residues affected by ADP (c) and ATP (d) binding are mapped onto the solution structure of the NTD of ScDpb5p using a backbone ribbon representative. The residues are colored according to the following scheme: $\Delta_{av}/\Delta_{max} < 0.23$ in gray, $0.23 \le \Delta_{av}/\Delta_{max} \le 0.46$ in orange, and $\Delta_{av}/\Delta_{max} > 0.46$ in red. The average Δ_{av}/Δ_{max} value over all the residues is 0.23, which is the same for the ADP and ATP titrations. Residues of which peaks disappear upon ATP/ADP binding are shown in yellow. Residues without backbone assignment and residues that could not be unambiguously assigned upon binding are shown in green.

When 0.1 mM ^{15}N-labeled NTD (residues 71–296) was titrated with ADP (ranging from 0.02 to 4.0 mM) in the presence of 5 mM MgCl$_2$, some cross peaks displayed progressive chemical shift changes and several cross peaks totally disappeared, while most cross peaks were slightly affected (Supplementary Fig. S2) in the ^{1}H–^{15}N HSQC spectra. This indicates that the binding of ADP to the NTD is weak and that the ADP-bound and ADP-free forms exchange in the fast and intermediate exchange regimes on the NMR timescale. Taking the advantage of NMR backbone assignments, we obtained the chemical shift perturbations for different amino acid residues by tracing the progressive chemical shift changes (shown in Fig. 3a). The same titration experiments were performed using ATP (concentration from 0.01 to 3.9 mM), and similar results were obtained (Fig. 3b). The similar patterns of the chemical shift perturbation show that ADP and ATP seem to bind to the NTD of ScDbp5p in a similar manner. Fitting the titration data to a simple 1:1 binding model (Supplementary Fig. S3), we estimated the binding affinity (K_d). For ADP, the K_d values obtained from different residues range from ~400 to ~570 μM. For ATP, the K_d values range from ~1.2 to ~1.5 mM.

Significant chemical shift changes and peak disappearance upon ATP/ADP binding were observed in four regions: A91–T154, A169–K187, E240–D252, and L269–T296. A small chemical shift change upon ATP binding was detected for A78 in the N-terminal part. Mapping of the chemical shift perturbations on the NTD structure of ScDbp5p (Fig. 3c and d) clearly shows not only that the residues around the consensus nucleotide binding motifs (motifs Q, I, and II) are affected by ADP and ATP binding but also that the residues far away in both sequence and space from the binding site are perturbed. On the basis of the chemical shift perturbations, it is difficult to define the exact ATP/ADP binding site. However, it is very likely that the binding site of ScDbp5p is similar to those of other DEAD-box proteins since the residues in the binding site (motifs Q, I, and II) are conserved. Interestingly, motif III, which does not interact with AMPPNP in VASA or with ADP in HuDbp5p, also displays significant chemical shift perturbation upon ligand binding. Moreover, many residues located at α3 and α6, which surround the binding site and form the edge of the biding site, display significant chemical shift changes too. These results imply the structural plasticity of the binding site of ScDbp5p. In TthDEAD/AMP[24] and UAP56/ADP[14] complexes, the concerted movement of helicase motifs (I, II, and III) was also observed upon nucleotide binding based on crystal structures.[24] Chemical shift perturbations of many residues far away in both sequence and space from the binding site also indicate that ATP/ADP binding may induce conformational changes of the entire domain. This result, together with the structural differences between SpDbp5p and HuDbp5p, strongly argues that the N-terminal flanking region of HuDbp5p undergoes a dramatic conformational change to interact with the main body of the NTD upon its binding to ADP. The NTD and CTD of Dbp5p do not interact with each other in the absence of their binding partners, but their interactions do exist in the presence of ADP. Therefore, it is tempting to speculate that ligand-induced conformational changes may enhance the interaction between the NTD and CTD and may further allow both the NTD and CTD to effectively interact with RNA. Such conformational changes have been observed in eIF4AIII too.[33]

In conclusion, the solution structure of ScDbp5p and the crystal structure of SpDbp5p reveal a significant structural similarity to other DEAD-box proteins and some novel structural characteristics for the two proteins studied here. SpDbp5p contains two RecA-like domains that do not interact with each other in the absence of RNA. NMR results show that the N-terminal flanking region of ScDpbp5p (M1–E70) is intrinsically unstructured and the region Y71–LR121 including the Q motif is highly dynamic on millisecond–microsecond timescales in solution. The dynamics and flexibility may allow the protein to interact with different substrates. The C-terminal flanking region of ScDbp5p forms a short β-strand and a long helix. This helix is unique for ScDbp5p and has not been observed in other DEAD-box proteins. NMR structure reveals that the extra insert in Dbp5p is located in a solvent-exposed loop that is capable of interacting with unidentified binding partners. NMR titrations showed that ADP and ATP bind to NTD only, consistent with the previous X-ray structural data of HuDbp5p. In response to the ADP binding, the N-terminal flanking region and even the entire NTD undergo large conformational changes. This conformational rearrangement may enhance nucleotide binding to the NTD and allow Dbp5p to adopt a closed conformation, which is more effective for binding to RNA.

PDB accession code

Coordinates for the solution structures of NTD and CTD of ScDbp5p and the crystal structure of SpDbp5p have been deposited in the PDB with accession codes 2kbe, 2kbf, and 3fho, respectively.

Supplementary Data

Supplementary data associated with this article can be found, in the online version, at doi:10.1016/j.jmb.2009.03.004

References

1. Chang, T. H., Arenas, J. & Abelson, J. (1990). Identification of five putative yeast RNA helicase genes. *Proc. Natl Acad. Sci. USA*, **87**, 1571–1575.

2. Amberg, D. C., Goldstein, A. L. & Cole, C. N. (1992). Isolation and characterization of RAT1: an essential gene of *Saccharomyces cerevisiae* required for the efficient nucleocytoplasmic trafficking of mRNA. *Genes Dev.* **6**, 1173–1189.

3. Tseng, S. S., Weaver, P. L., Liu, Y., Hitomi, M., Tartakoff, A. M. & Chang, T. H. (1998). Dbp5p, a cytosolic RNA helicase, is required for poly(A)+RNA export. *EMBO J.* **17**, 2651–2662.

4. Snay-Hodge, C. A., Colot, H. V., Goldstein, A. L. & Cole, C. N. (1998). Dbp5p/Rat8p is a yeast nuclear pore-associated DEAD-box protein essential for RNA export. *EMBO J.* **17**, 2663–2676.

5. Hodge, C. A., Colot, H. V., Stafford, P. & Cole, C. N. (1999). Rat8p/Dbp5p is a shuttling transport factor that interacts with Rat7p/Nup159p and Gle1p and suppresses the mRNA export defect of xpo1-1 cells. *EMBO J.* **18**, 5778–5788.

6. Schmitt, C., von Kobbe, C., Bachi, A., Pante, N., Rodrigues, J. P., Boscheron, C. *et al.* (1999). Dbp5, a DEAD-box protein required for mRNA export, is recruited to the cytoplasmic fibrils of nuclear pore complex via a conserved interaction with CAN/Nup159p. *EMBO J.* **18**, 4332–4347.

7. Strahm, Y., Fahrenkrog, B., Zenklusen, D., Rychner, E., Kantor, J., Rosbach, M. & Stutz, F. (1999). The RNA export factor Gle1p is located on the cytoplasmic fibrils of the NPC and physically interacts with the FG-nucleoporin Rip1p, the DEAD-box protein Rat8p/Dbp5p and a new protein Ymr 255p. *EMBO J.* **18**, 5761–5777.

8. Lund, M. K. & Guthrie, C. (2005). The DEAD-box protein Dbp5p is required to dissociate Mex67p from exported mRNPs at the nuclear rim. *Mol. Cell*, **20**, 645–651.

9. Gross, T., Siepmann, A., Sturm, D., Windgassen, M., Scarcelli, J. J., Seedorf, M. *et al.* (2007). The DEAD-box RNA helicase Dbp5 functions in translation termination. *Science*, **315**, 646–649.

10. Scarcelli, J. J., Viggiano, S., Hodge, C. A., Heath, C. V., Amberg, D. C. & Cole, C. N. (2008). Synthetic genetic array analysis in *Saccharomyces cerevisiae* provides evidence for an interaction between RAT8/DBP5 and genes encoding P-body components. *Genetics*, **179**, 1945–1955.

11. Weirich, C. S., Erzberger, J. P., Flick, J. S., Berger, J. M., Thorner, J. & Weis, K. (2006). Activation of the DExD/H-box protein Dbp5 by the nuclear-pore protein Gle1 and its coactivator InsP6 is required for mRNA export. *Nat. Cell Biol.* **8**, 668–676.

12. Alcazar-Roman, A. R., Tran, E. J., Guo, S. & Wente, S. R. (2006). Inositol hexakisphosphate and Gle1 activate the DEAD-box protein Dbp5 for nuclear mRNA export. *Nat. Cell Biol.* **8**, 711–716.

13. Story, R. M., Li, H. & Abelson, J. N. (2001). Crystal structure of a DEAD box protein from the hyperthermophile *Methanococcus jannaschii*. *Proc. Natl Acad. Sci. USA*, **98**, 1465–1470.

14. Shi, H., Cordin, O., Minder, C. M., Linder, P. & Xu, R. M. (2004). Crystal structure of the human ATP-dependent splicing and export factor UAP56. *Proc. Natl Acad. Sci. USA*, **101**, 17628–17633.

15. Caruthers, J. M., Johnson, E. R. & McKay, D. B. (2000). Crystal structure of yeast initiation factor 4A, a DEAD-box RNA helicase. *Proc. Natl Acad. Sci. USA*, **97**, 3080–3085.

16. Cheng, Z., Coller, J., Parker, R. & Song, H. (2005). Crystal structure and functional analysis of DEAD-box protein Dhh1p. *RNA*, **11**, 1258–1270.

17. Sengoku, T., Nureki, O., Nakamura, A., Kobayashi, S. & Yokoyama, S. (2006). Structural basis for RNA unwinding by the DEAD-box protein *Drosophila* Vasa. *Cell*, **125**, 287–300.

18. Högbom, M., Collins, R., van den Berg, S., Jenvert, R. M., Karlberg, T., Kotenyova, T. *et al.* (2007). Crystal structure of conserved domains 1 and 2 of the human DEAD-box helicase DDX3X in complex with the mononucleotide AMP. *J. Mol. Biol.* **372**, 150–159.

19. Johnson, E. R. & McKay, D. B. (1999). Crystallographic structure of the amino terminal domain of yeast initiation factor 4A, a representative DEAD-box RNA helicase. *RNA*, **5**, 1526–1534.

20. Benz, J., Trachsel, H. & Baumann, U. (1999). Crystal structure of the ATPase domain of translation initiation factor 4A from *Saccharomyces cerevisiae*—the prototype of the DEAD box protein family. *Structure*, **7**, 671–679.

21. Zhao, R., Shen, J., Green, M. R., MacMorris, M. & Blumenthal, T. (2004). Crystal structure of UAP56, a DExD/H-box protein involved in pre-mRNA splicing and mRNA export. *Structure*, **12**, 1373–1381.

22. Kurimoto, K., Muto, Y., Obayashi, N., Terada, T., Shirouzu, M., Yabuki, T. *et al.* (2005). Crystal structure of the N-terminal RecA-like domain of a DEAD-box RNA helicase, the *Dugesia japonica* vasa-like gene B protein. *J. Struct. Biol.* **150**, 58–68.

23. Carmel, A. B. & Matthews, B. W. (2004). Crystal structure of the BstDEAD N-terminal domain: a novel DEAD protein from *Bacillus stearothermophilus*. *RNA*, **10**, 66–74.

24. Rudolph, M. G., Heissmann, R., Wittmann, J. G. & Klostermeier, D. (2006). Crystal structure and nucleotide binding of the *Thermus thermophilus* RNA helicase Hera N-terminal domain. *J. Mol. Biol.* **361**, 731–743.

25. Liu, D., Wang, Y. S., Gesell, J. J. & Wyss, D. F. (2001). Solution structure and backbone dynamics of an engineered arginine-rich subdomain 2 of the hepatitis C virus NS3 RNA helicase. *J. Mol. Biol.* **314**, 543–561.

26. Xu, Y., Zheng, Y., Fan, J. S. & Yang, D. (2006). A novel strategy for structure determination of large proteins without deuteration. *Nat. Methods*, **3**, 931–937.

27. Xu, Y., Long, D. & Yang, D. (2007). Rapid data collection for protein structure determination by NMR spectroscopy. *J. Am. Chem. Soc.* **129**, 7722–7723.

28. Cornilescu, G., Delaglio, F. & Bax, A. (1999). Protein backbone angle restraints from searching a database for chemical shift and sequence homology. *J. Biomol. NMR*, **13**, 289–302.

29. Story, R. M. & Steitz, T. A. (1992). Structure of the recA protein–ADP complex. *Nature*, **355**, 374–376.

30. Cordin, O., Banroques, J., Tanner, N. K. & Linder, P. (2006). The DEAD-box protein family of RNA helicases. *Gene*, **367**, 17–37.

31. Rollenhagen, C., Hodge, C. A. & Cole, C. N. (2004). The nuclear pore complex and the DEAD box protein Rat8p/Dbp5p have nonessential features which appear to facilitate mRNA export following heat shock. *Mol. Cell. Biol.* **24**, 4869–4879.

32. Bono, F., Ebert, J., Lorentzen, E. & Conti, E. (2006). The crystal structure of the exon junction complex

reveals how it maintains a stable grip on mRNA. *Cell*, **126**, 713–725.

33. Andersen, C. B., Ballut, L., Johansen, J. S., Chamieh, H., Nielsen, K. H., Oliveira, C. L. *et al.* (2006). Structure of the exon junction core complex with a trapped DEAD-box ATPase bound to RNA. *Science*, **313**, 1968–1972.

34. Yang, D., Zheng, Y., Liu, D. & Wyss, D. F. (2004). Sequence specific assignments of methyl groups in high molecular weight proteins. *J. Am. Chem. Soc.* **126**, 3710–3711.

35. Zheng, Y., Giovannelli, J. L., Ho, N. T., Ho, C. & Yang, D. (2004). Side chain assignments of methyl-containing residues in a uniformly 13C-labeled hemoglobin in the carbonmonoxy form. *J. Biomol. NMR*, **30**, 423–429.

36. Delaglio, F., Grzesiek, S., Vuister, G. W., Zhu, G., Pfeifer, J. & Bax, A. (1995). NMRPipe: a multidimensional spectral processing system based on UNIX pipes. *J. Biomol. NMR*, **6**, 277–293.

37. SPARKY (v.3.106) (T. D. Goddard & D. G. Kneller, University of California, San Francisco).

38. Schwieters, C. D., Kuszewski, J. J., Tjandra, N. & Clore, G. M. (2003). The Xplor-NIH NMR molecular structure determination package. *J. Magn. Reson.* **160**, 66–74.

39. Laskowski, R. A., Rullmannn, J. A., MacArthur, M. W., Kaptein, R. & Thornton, J. M. (1996). AQUA and PROCHECK-NMR: programs for checking the quality of protein structures solved by NMR. *J. Biomol. NMR*, **8**, 477–486.

40. Koradi, R., Billeter, M. & Wuthrich, K. (1996). MOLMOL: a program for display and analysis of macromolecular structures. *J. Mol. Graphics*, **14**, 32–51.

41. Collaborative Computational Project, No. 4 (1994). The CCP4 suite: programs for protein crystallography. *Acta Crystallogr., Sect. D: Biol. Crystallogr.* **50**, 760–763.

42. McCoy, A. J., Grosse-Kunstleve, R. W., Adams, P. D., Winn, M. D., Storoni, L. C. & Read, R. J. (2007). Phaser crystallographic software. *J. Appl. Crystallogr.* **40**, 658–674.

43. Murshudov, G. N., Vagin, A. A. & Dodson, E. J. (1997). Refinement of macromolecular structures by the maximum-likelihood method. *Acta Crystallogr., Sect. D: Biol. Crystallogr.* **53**, 240–255.